Pronounced Conversion of the Metal-Specific Activity of Superoxide Dismutase from *Porphyromonas gingivalis* by the Mutation of a Single Amino Acid (Gly155Thr) Located Apart from the Active Site[†,‡]

Fumiyuki Yamakura,[*,§,||] Shigetoshi Sugio,[||,⊥] B. Yukihiro Hiraoka,[||,@] Daijiro Ohmori,[§] and Takehiro Yokota[⊥]

Department of Chemistry, Juntendo University School of Medicine, Inba 270-1695, Japan, Science & Technology Research Center, Mitsubishi Chemical Corporation, 1000 Kamoshida, Aoba, Yokohama 227-8502, Japan, and Institute for Oral Science, Matsumoto Dental University, Shiojiri 399-0781, Japan

Received June 4, 2003; Revised Manuscript Received July 30, 2003

ABSTRACT: Glycine 155, which is located ∼10 Å from the active metal sites, is mostly conserved in aligned amino acid sequences of manganese-specific superoxide dismutases (Mn-SODs) and cambialistic SOD (showing the same activity with Fe and Mn) from *Porphyromonas gingivalis*, but is substituted for threonine in most Fe-SODs. Since Thr155 is located between Trp123 and Trp125, and Trp123 is one member of the metal-surrounding aromatic amino acids, there is a possibility that the conversion of this amino acid may cause a conversion of the metal-specific activity of cambialistic *P. gingivalis* SOD. To clarify this possibility, we have prepared a mutant of the *P. gingivalis* SOD with conversion of Gly155 to Thr. The ratios of the specific activities of Fe- to Mn-reconstituted enzyme, which are measured by the xanthine oxidase/cytochrome *c* method, increased from 0.6 in the wild-type to 11.2 in the mutant SODs, indicating the conversion of the metal-specific activity of the enzyme from a cambialistic type to an Fe-specific type. The visible absorption spectra of the Fe- and Mn-reconstituted mutant SODs closely resembled those of Fe-specific SOD. Furthermore, the EPR spectra of the Fe- and Mn-reconstituted mutant SODs also closely resembled those of Fe-specific SOD. Three-dimensional structures of the Fe-reconstituted wild-type SOD and Mn-reconstituted mutant SOD have been determined at 1.6 Å resolution. Both structures have identical conformations, orientations of residues involved in metal binding, and hydrogen bond networks, while the side chain of Trp123 is moved further toward the metal-binding site than in wild-type SOD. A possible contribution of the structural differences to the conversion of the metal-specific activity through rearrangement of the hydrogen bond network among Trp123, Gln70, Tyr35, and the metal-coordinated solvent is discussed.

Four main classes of superoxide dismutase (SOD)[1] have been reported, each differing in their metallic cofactors: copper- and zinc-containing (Cu,Zn-SOD), iron-containing (Fe-SOD), manganese-containing (Mn-SOD), and nickel-containing (Ni-SOD) SODs. Among these SODs, Fe-SOD and Mn-SOD can be divided into two types based on metal specificity for the enzymatic reaction. The first is a metal-specific type of SOD, which requires the original metals for the activity; that is, manganese-substituted Fe-SODs (*1*) and iron-substituted Mn-SODs (*2*, *3*) retain little or no enzymatic activity. Fe-SOD from *Pseudomonas ovalis* (*1*) and Fe- and Mn-SOD from *Escherichia coli* (*2*, *3*) are typical examples of this type of SOD. The other type of SOD, cambialistic SOD (*4*−*7*), uses both metals to exhibit the enzymatic activity. Despite these differences in metal specificity, Mn-SODs (*8*−*10*), Fe-SODs (*11*, *12*), and cambialistic SODs (*13*, *14*) have a large degree of sequence homology and X-ray structural similarity. The iron and manganese atoms are commonly ligated by three histidine residues, one aspartate residue, and one solvent molecule. Since both Fe and Mn can mediate dismutation reactions of superoxide, and since specificity of metals can be different according to the type of SODs, there must be some subtle but critical differences in the interaction between the proteins and the metal ion. Therefore, Fe- and Mn-SODs provide an ideal model for analyzing how a metalloenzyme precisely tunes its metal site suitably for metal−substrate interaction.

Although no significant difference has been observed at the active site of these SODs, two minor differences were observed in the second sphere of the active site (within 8 Å) of the enzymes. One difference is that Gln70 in Fe-SODs is complementarily substituted with Gln142 in Mn-SODs (note that the amino acid numbering is based on the positions in *Porphyromonas gingivalis* SOD), with the same orienta-

[†] This work was partially supported by the National Project on Protein Structural and Functional Analyses run by the Japanese Ministry of Education, Culture, Sports, Science and Technology.

[‡] PDB entries 1UER for the wild-type Fe-SOD and 1UES for the mutant Mn-SOD.

* To whom correspondence should be addressed. Telephone: +81-476-98-1001. Fax: +81-476-98-1011. E-mail: yamakura@sakura.juntendo.ac.jp.

[§] Juntendo University School of Medicine.

[||] These authors contributed equally to this work.

[⊥] Mitsubishi Chemical Corp.

[@] Matsumoto Dental University.

[1] Abbreviations: SOD, superoxide dismutase; Fe-SOD, iron-containing superoxide dismutase; Mn-SOD, manganese-containing superoxide dismutase; MBP, maltose binding protein.

10.1021/bi0349625 CCC: $25.00
Published on Web 08/21/2003

tion of the side chain amide groups of the glutamine residues. These amide groups are part of a hydrogen bond network that includes conserved Tyr35 and the metal−ligand solvent, and they may involve this tyrosine in catalysis at the metal in the Fe- and Mn-SODs (*8*−*14*). The second difference is that Tyr77 in Fe-SODs is changed to Phe in Mn-SODs (*8*−*14*). Among these two differences, the second difference does not contribute to the metal-specific activity of Fe- and Mn-SODs, since the substitution of Tyr77 with Phe in the metal-specific Fe-SOD from *Sulfolobus solfataricus* did not change the metal-specific activity of the enzyme (*15*).

The glutamine residue of a cambialistic SOD from *P. gingivalis* is located at position 70, the same as for the Fe-specific type SODs (*14*). Since no unique difference in the structure of the cambialistic SOD has been observed compared with Fe- and Mn-SODs, as described above, the metal-specific activities of the Fe- and Mn-SODs may also be controlled by a mechanism similar to that of the cambialistic SODs. Therefore, it is important to clarify the role of the positional difference of the glutamine residue in the metal-specific activity of *P. gingivalis* SOD by conversion of amino acids at positions 70 and 142 using site-directed mutagenesis. We prepared a mutant of the enzyme with conversions of Gln70 to Gly and Ala142 to Gln. We found that this exchange produced an increase in the Mn specificity of the enzymatic reaction (2.5-fold) and more resemblance of the visible absorption spectra to those of Mn-specific SOD (*16*). Schwartz *et al*. (*17*) also reported a similar result for the Mn-SOD form *E. coli*. They found that the enzymatic activity of the Fe-substituted Gly77Gln/Gln146Ala mutant enzyme was ∼7% of that of Fe-SOD, in contrast to the Fe-substituted wild-type Mn-SOD, which had 0% of Fe-SOD's activity. Since the conversion of the metal-specific activities of each mutant enzyme was only partial, the positional difference of the glutamine residue in the amino acid sequence is not the sole determinant of the metal-specific activity. Therefore, we direct our attention to the other amino acids that are not conserved between Fe- and Mn-SODs. Although most of these amino acids in *P. gingivalis* SOD are the same as Fe-specific SODs, a few of those amino acids are characteristic of Mn-specific SOD. We focused on Gly155, which is conserved as Thr in the most Fe-specific SODs, and Gly in the most Mn-specific SODs.

In this paper, we constructed Gly155Thr mutant SOD, reconstituted with Fe and Mn, analyzed the X-ray structures of the metal-reconstituted enzymes, and determined some properties of the enzymes. We found that this mutation changes the metal-specific activity remarkably from a cambialistic type to one close to an Fe-specific type. This is the first successful report for the Fe- and Mn-SOD family of changing the metal-specific activity not only drastically but also by site-directed mutagenesis of an amino acid other than an active site or second sphere. We proposed a possible mechanism for the changing of the metal-specific activity from the comparison of the X-ray structures of the wild-type and mutant SODs.

MATERIALS AND METHODS

Materials. The vector pMAL-c2, amylose resin, and *E. coli* strain TB-1 were obtained from New England Biolabs. Cytochrome *c* and xanthine oxidase were obtained from Sigma and Roche Diagnostics, respectively.

Site-Directed Mutagenesis of SOD. Construction of the expression vector, overexpression, and purification of the MBP−SOD fusion protein were carried out by the method described previously (*16*). Briefly, the coding *sod* gene was inserted downstream of the *malE* gene of *E. coli*, which encodes the maltose-binding protein (MBP), resulting in the expression of a MBP−SOD fusion protein. The transformed *E. coli* was grown in a rich broth medium. After the fusion protein was isolated from the supernatant of the cells by an amylose resin column, the eluted protein was digested with trypsin. SOD was further purified from the digests by using a Q-Sepharose column (Amersham Biosciences) to produce a single band by SDS−PAGE. Purified SOD was obtained at a level of ∼15−20 mg/L of culture. The *Eco*RI−*Hin*dIII fragment of *SOD*/pMal-c2, which corresponds to nucleotides 76−573 of the *sod* sequence, was ligated into M13mp19 for mutagenesis. *In vitro* mutagenesis of SOD was performed using the Mutan-K system (Takara Biomedicals, Tokyo, Japan), which is based on the method described by Kunkel (*18*) under conditions recommended by the manufacturer. A substitution of Gly (GGA) with Thr (ACA) was introduced at amino acid position 155. Mutant cDNA was screened and sequenced to ensure the absence of spurious mutations. Mutant SOD was expressed and purified by the same methods as the wild-type SOD described above.

Preparation of Metal-Reconstituted Proteins. Fe- and Mn-reconstituted wild-type and mutant SODs were prepared according to the acid−guanidine hydrochloride denaturation method described in a previous paper (*7*). To remove minor components in the reconstituted proteins, we used an HPLC system (Jusco 800) equipped with a hydroxyapatite column (Bio-Rad).

Crystallization and Structural Determination of Wild-Type and Mutant SODs. Purified enzymes were concentrated to 10 mg/mL. Fe-reconstituted wild-type SOD and Mn-reconstituted mutant SOD were crystallized with a solution of 25−30% (w/v) polyethylene glycol 4000 (PEG4000) in 100 mM potassium phosphate buffer (pH 5.8) by the hanging-drop vapor diffusion method at 293 K, and prismatic crystals with a typical size of 0.3 mm for each edge were grown within a few weeks. We obtained a few crystals of Mn-reconstituted wild-type SOD and Fe-reconstituted mutant SOD by the same methods as described above and the other conditions. However, the stability and quality of the crystals were markedly inferior to those of the wild-type Fe-SOD and mutant Mn-SOD, respectively, and did not exhibit sufficient diffractions in our data collection system described below.

Crystals were transferred to a cryoprotectant solution containing 30% (w/v) PEG4000 in 100 mM potassium phosphate buffer (pH 5.8) and flash-cooled in a nitrogen gas stream at 100 K. X-ray diffraction data from each crystal of Fe-SOD and Mn-SOD were collected by using synchrotron radiation at BL-24XU of SPring-8 equipped with an R-AXIS V imaging plate detector (Rigaku Co.). Intensity data were indexed and integrated using Mosflm (*19*). Subsequent data processing was done with the CCP4 suite (*20*). Crystals of wild-type Fe-SOD belong to orthorhombic space group $P2_12_12_1$ with a Matthews constant (*21*) of 2.13 Å^3/Da and the following unit cell constants: $a = 75.3$ Å, $b = 95.9$ Å, and $c = 101.4$ Å. Crystals of mutant Mn-SOD belong to orthorhombic space group $P2_12_12_1$ with a Matthews constant

Table 1: Data Collection and Reduction Statistics for Wild-Type Fe-SOD and the Gly155Thr Mutant Mn-SOD from *P. gingivalis*

	wild-type Fe-SOD	mutant Mn-SOD
crystal data		
space group	$P2_12_12_1$	$P2_12_12_1$
unit cell axes (Å)		
a	75.3	71.7
b	95.9	95.1
c	101.4	98.8
Z	16	16
intensity data statistics		
X-ray source	SPring-8	SPring-8
beamline	BL24XU	BL24XU
detector	R-AXIS V	R-AXIS V
wavelength (Å)	0.836	0.836
temperature (K)	100	100
resolution (Å)	1.5	1.5
no. of reflections	108296	84510
completeness (%)	98.0	76.0
redundancy	6.7	7.3
$\langle I \rangle$/SD	15.3	11.0
R_{merge} (%)	7.1	5.5
refinement statistics		
resolution (Å)	20.0−1.6	20.0−1.6
no. of reflections	91058	74648
completeness (%)	90.8	80.9
R-factor (%)	23.1	22.1
R_{free} (%)	25.6	25.0
no. of atoms (four molecules)		
SOD	6104	6116
ion	4	4
water	504	352
rmsd from ideal values		
distances (Å)	0.012	0.009
angles (deg)	1.509	1.463
improper angles (deg)	0.936	0.873
dihedral angles (deg)	24.24	24.04
bond restraints (Å^2)	0.413	0.474
angle restraints (Å^2)	0.710	0.809

(*21*) of 1.96 Å^3/Da with the following unit cell constants: $a = 71.7$ Å, $b = 95.1$ Å, and $c = 98.8$ Å. Crystal data and intensity statistics are summarized in Table 1.

The initial phases set at 1.6 Å resolution were determined by molecular replacement with the structure of *P. gingivalis* Fe-SOD at 1.8 Å resolution [PDB entry 1QNN (*14*)] as a probe model, using X-PLOR98.1 (*22*). The models were refined using X-PLOR98.1, and model building and fitting were done with XtalView (*23*). The final structure of wild-type Fe-SOD gave a crystallographic *R*-factor of 0.23 and a free *R*-factor of 0.26. A Ramachandran plot (*24*) indicates that backbone torsion angles for most non-glycine residues fall within the favorable and the acceptable regions, with the exception of Lys85 and Asn141. The rmsd's from the ideal values are 0.012 Å for bond lengths and 1.509° for bond angles. There are four (two dimers) Fe-SOD molecules in the asymmetric unit, together with 504 water molecules and four iron atoms. The final structure of mutant Mn-SOD gave a crystallographic *R*-factor of 0.22 and a free *R*-factor of 0.25. A Ramachandran plot indicates that backbone torsion angles for most non-glycine residues fall within the favorable and the acceptable regions with the exception of Lys85, Asn141, and Gln168. The rmsd's from the ideal values are 0.009 Å for bond lengths and 1.463° for bond angles. There are four Mn-SOD molecules together with 352 water molecules and four manganese atoms. These refinement statistics are summarized in Table 1.

The atomic coordinates of wild-type Fe-SOD and mutant Mn-SOD have been deposited in the Protein Data Bank as entries 1UER and 1UES, respectively.

Analytical Methods. The molecular masses of the mutant SODs were determined with an SSQ 7000 electrospray ionization mass spectrometer (Thermo-Quest Finnigan Mat Co.). The analytical conditions were as follows: spray voltage of 4.5 kV, electron multiplier voltage of 1200 V, manifold vacuum of 7.0×10^{-6}, manifold temperature of ~70 °C, capillary temperature of 200 °C, scan range of *m*/*z* 500−2500, and scan time of 5 s. The SODs were dissolved in a mixture of methanol and 0.5% acetic acid (1:1, v/v) to a final concentration of 20 pmol/μL and infused into the ion source of the SSQ 7000 spectrometer with a pump. SOD activity was measured by inhibition of the xanthine/xanthine oxidase-induced reduction of cytochrome *c* at pH 7.8 (*25*), with reduction of the final volume of the assay system from 3 to 0.75 mL (*7*). Metal contents were determined by using atomic absorption spectrometry with a Hitachi Z-9000 atomic absorption spectrophotometer. Protein concentrations of Fe- and Mn-reconstituted mutant *P. gingivalis* SOD were estimated by using molar absorption coefficients of 69 800 and 70 100 M^{-1} cm^{-1} at 280 nm, respectively, which were measured by the BCA method of Smith *et al.* (*26*) using bovine serum albumin as a standard. EPR spectra were obtained on a JEOL JES-FE3XG spectrometer equipped with an RMS model CT-470-ESR cryostat system and a Scientific Instruments model 9650 temperature controller. Magnetic field measurements for *g* value determinations were taken with a JEOL ES-FC4 NMR gaussmeter.

RESULTS

Characterization of the Mutant SODs. Gly155Thr mutant SOD was screened and sequenced to ensure the absence of spurious mutations, and additionally subjected to mass spectroscopy to measure an accurate molecular mass. Deconvolution of the protein mass spectrum revealed a molecular mass of 21 546 Da, which was almost consistent with the calculated value for the SOD (21 545 Da). The difference between the observed molecular mass and calculated molecular mass of wild-type SOD (21 501 Da), 45 Da, was close to that between the calculated value of the replacement of glycine and threonine (44 Da) in the protein structure. These data show that the construction of the plasmid, the mutation of the *sod* gene, and the purification of the SOD occurred as intended. After the purified mutant SODs were reconstituted with iron or manganese, they were subjected to nondenaturing PAGE along with the wild-type SODs. Each of the mutant and wild-type SODs gave a single major band (>95%) and a faster moving minor band (<5%), with the same motilities for each sample.

Structures of Fe-Reconstituted Wild-Type SOD and Mn-Reconstituted Mutant SOD. The current atomic coordinates give an *R* of 0.23 and an R_{free} of 0.26 for Fe-reconstituted Fe-SOD and an *R* of 0.22 and an R_{free} of 0.25 for Mn-reconstituted mutant SOD against all the reflections in the resolution range of 50.0−1.60 Å. The current structure reveals reasonably small rms deviations from the ideal bond distances, angles, and torsion angles (data not shown). No serious geometrical defects on either main chain or side chain properties were observed from the analysis with PROCHECK

Table 2: Bond Distances and Angles between the Active Site Metals and the Five Ligands in the Wild-Type Fe-SOD and the Mutant Mn-SOD

	Mol-1	Mol-2	Mol-3	Mol-4
Wild-Type SOD				
	Distances (Å)			
Fe−His27	2.24	2.26	2.25	2.26
Fe−His74	2.17	2.19	2.23	2.23
Fe−Asp157	1.98	2.04	1.97	2.05
Fe−His161	2.24	2.25	2.21	2.19
Fe−OH^- (H_2O)	2.04	2.09	2.01	2.18
	Angles (deg)			
His27−Fe−His74	83.19	84.02	80.82	82.62
His27−Fe−Asp157	88.40	85.37	89.47	88.11
His27−Fe−His161	94.35	97.77	93.27	98.00
His27−Fe−OH^- (H_2O)	177.17	175.76	177.20	170.06
His74−Fe−Asp157	111.91	112.75	111.88	113.86
His74−Fe−His161	130.77	129.41	127.88	130.88
His74−Fe−OH^- (H_2O)	99.18	95.38	96.39	95.78
Asp157−Fe−His161	117.18	117.80	119.85	115.25
Asp157−Fe−OH^- (H_2O)	89.27	91.02	91.75	83.57
His161−Fe−OH^- (H_2O)	85.29	85.86	88.30	90.47
Mutant G155T SOD				
	Mol-1	Mol-2	Mol-3	Mol-4
	Distances (Å)			
Mn−His27	2.19	2.22	2.17	2.25
Mn−His74	2.20	2.23	2.17	2.24
Mn−Asp157	2.07	2.10	2.07	1.99
Mn−His161	2.23	2.22	2.17	2.31
Mn−H_2O	2.24	2.09	2.12	2.25
	Angles (deg)			
His27−Mn−His74	93.81	88.93	89.04	92.2
His27−Mn−Asp157	87.33	85.10	86.26	86.53
His27−Mn−His161	91.51	94.37	90.11	94.03
His27−Mn−H_2O	173.16	172.48	177.21	172.09
His74−Mn−Asp157	114.99	115.14	115.84	115.62
His74−Mn−His161	123.42	124.00	125.25	123.62
His74−Mn−H_2O	88.40	89.37	91.49	90.14
Asp157−Mn−His161	121.52	120.84	118.71	120.66
Asp157−Mn−H_2O	85.87	89.00	91.05	85.65
His161−Mn−H_2O	92.67	92.66	91.82	90.95

(*27*). The mean error in atomic coordinates (*26*) was evaluated at 0.18 Å based on R (0.24 Å based on R_{free}). Each subunit of the wild-type and mutant *P. gingivalis* SODs exhibited almost the same polypeptide folding as purified wild-type SOD shown in a previous paper (*14*). Bond distances and angles for the active site metals and the five coordinated atoms in each of the four molecules of the wild-type Fe-SOD and the mutant Mn-SOD in the asymmetric unit are summarized in Table 2. Statistically, no significant differences in the bond distances and angles were observed between the wild-type Fe-SOD and the mutant Mn-SOD, except that the His74−Fe−H_2O(OH^-) bond angle was slightly larger than the His−Mn−H_2O bond angle. Although the differences are statistically not significant, the average bond distances between the active site metals and the five coordinated atoms in each of the four SOD molecules in asymmetric units are longer in the mutant Mn-SOD than in wild-type Fe-SOD (0.01−0.13 Å, Table 2). Since the valency of manganese in the mutant Mn-SOD seems to be Mn^{2+} and that of iron in the wild-type Fe-SOD seems to be Fe^{3+} from the data of EPR and absorption spectra (Figures 3−5), the longer average bond distances in the mutant Mn-SOD can be attributed to the shorter ionic radius of Mn^{2+} (0.64 Å) versus Fe^{3+} (0.80 Å) (*28*). In addition, no significant difference was observed among amino acid residues surrounding active site metals between the wild-type and mutant enzymes, as shown in Figure 1. However, we found one major difference and a few minor differences between the wild-type Fe-SOD and the mutant Mn-SOD. The major difference was that the side chain of the mutated Thr155 was positioned between Trp123 and Trp125; thereby, Trp123 was moved toward the active site metal, and Trp125 was moved to the other side. Accompanying this change was rearrangement of the hydrogen bond network. In the wild-type enzyme, OE1 of Gln70 makes a weak hydrogen bond to ND2 of Asn73. However, this distance was extended from 3.33 to 3.56 Å, and the hydrogen bond might be lost in the mutant enzyme. The mutant enzyme, instead, possibly made another weak hydrogen bond between ND2 of Asn73 and NE1 of Trp123 (3.22 Å). In addition to this difference, an extension of the distance between NE2 of Gln70 and the coordinated solvent was observed, from 2.93 Å in the wild-type enzyme to 3.37 Å in the mutant enzyme (Figure 2).

Catalytic Properties. Table 3 shows the specific activities and metal contents of the Fe-reconstituted and Mn-reconstituted wild-type and mutant SODs. Each metal-reconstituted SOD contained nearly stoichiometric amounts of iron or manganese and negligible amounts of the other metals, suggesting that each metal-reconstituted enzyme contained negligible amounts of nonspecific binding metals. To correct for the influence of different metal contents on the apparent activity of each of the SOD preparations, we divided the specific activities of the SODs expressed in units per milligram of protein by the moles of Fe and/or Mn per mole of subunit. The wild-type Fe- and Mn-SODs exhibited similar specific activities as described previously (*7*). The ratios of the specific activities of Fe-SOD to Mn-SOD were 0.60 in the wild-type SOD and 11.2 in the mutant SOD. Therefore, we conclude that the metal-specific activity of *P. gingivalis* SOD was changed from a cambialistic type to an Fe-specific type by the Gly155Thr mutation.

Spectroscopic Properties. To evaluate the differences in the metal sites, we compared the visible absorption spectra of the Fe-reconstituted and Mn-reconstituted wild-type and mutant SODs (Figure 3A,B). The visible absorption spectra of Fe-SOD from *Ps. ovalis* (spectrum 2 in panel A) and both Fe-substituted and native *Serratia marcescens* Mn-SOD (spectra 1 in panels A and B), which are metal-specific SODs (*1*, *29*), are also shown in panels A and B as a comparison. As shown in panel A, the mutant Fe-SOD has a spectrum that very closely resembles that of Fe-specific Fe-SOD from *Ps. ovalis*. However, the wild-type Fe-SOD spectrum is intermediate between those of the Fe-specific SOD type and the Fe-substituted Mn-specific SOD type. Although the shapes of the spectra of the wild-type Mn-SOD and Gly155Thr mutant Mn-SOD were almost the same as that of the Mn-specific Mn-SOD, the extinction coefficients of the peak absorption at 480 nm were 258 M^{-1} cm^{-1} for the wild-type Mn-SOD and 55 M^{-1} cm^{-1} for the mutant Mn-SOD, which were only $\sim 1/4.7$ and $\sim 1/10.4$ of the extinction coefficient of the Mn-specific Mn-SOD (573 M^{-1} cm^{-1}), respectively. Since Mn-substituted Fe-specific Fe-SODs exhibited almost no or very weak absorption around 480 nm (*30*, *31*), the Mn-reconstituted mutant enzyme is assumed to closely resemble the Fe-SOD.

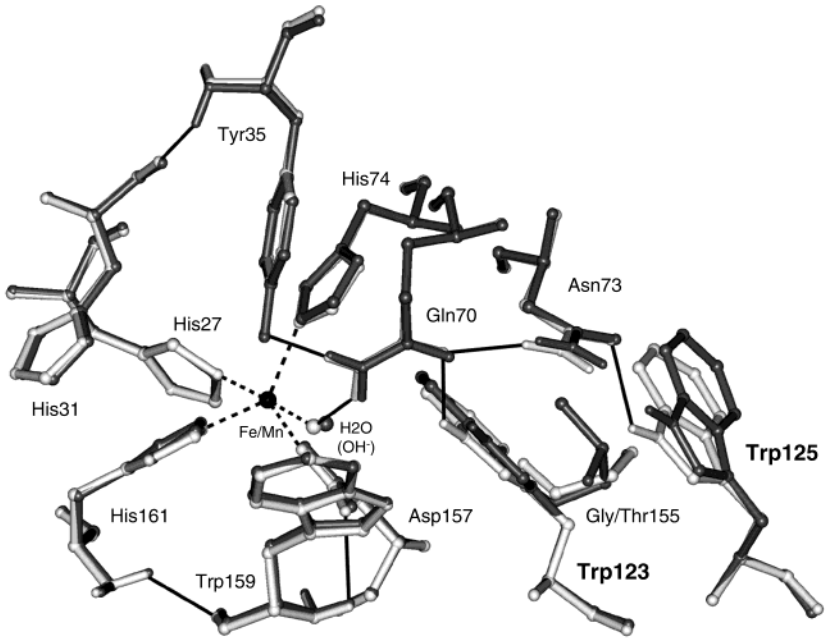

FIGURE 1: Structural comparison between wild-type and mutant SODs at the metal-binding site. Residues of the wild-type and mutant SODs are shown in gray and black sticks, respectively. Metal ions, Fe(III) and Mn(II/III), are shown as black balls, and water molecules are shown as white and gray balls. The dashed lines represent coordinate bonds, and the solid lines represent hydrogen bonds in the wild-type SOD. The orientation of residues corresponding to metal binding (His27, His74, Asp157, and His161, dashed line) is completely conserved in both structures, while the side chain of Trp123 is moved toward the metal-binding site and that of Trp125 moved away. This figure was drawn by using ACCELRYS Viewer Lite version 4.2.

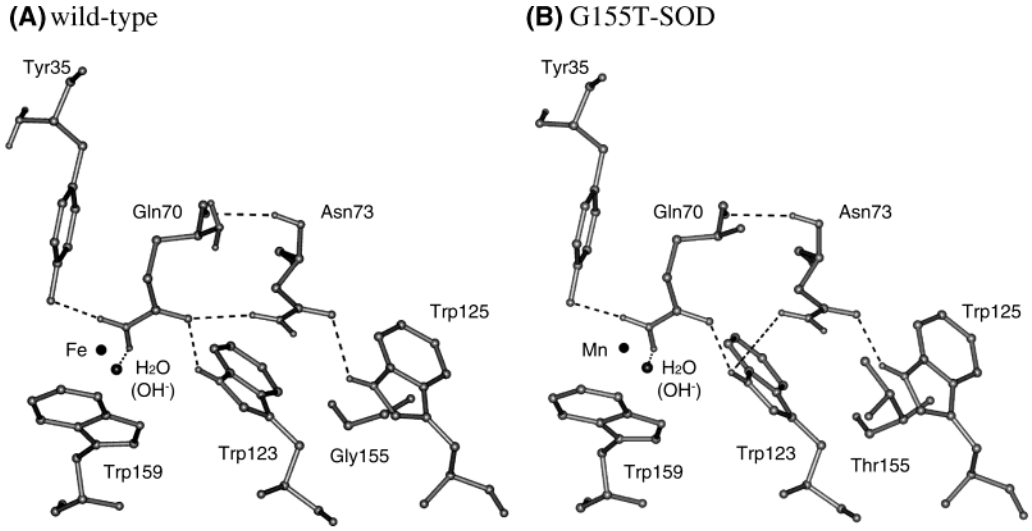

FIGURE 2: Hydrogen bond networks of wild-type Fe-SOD (A) and mutant Mn-SOD (B). Residues corresponding to a hydrogen bond network are completely conserved in both structures. The only distinction between the wild-type and mutant SODs is the hydrogen bond formed at OE1 of Gln70 and ND2 of Asn73. The bond stabilizes the side chain of Gln70. This figure was drawn by using ACCELRYS Viewer Lite version 4.2.

Figure 4 shows EPR signals of the wild-type and Gly155Thr mutant Fe-SOD from *P. gingivalis* at pH 7.7 and 4.4 K, along with those of Fe-specific Fe-SOD (*Ps. ovalis*) (*1*) at pH 7.8 and 8.8 K and Fe-substituted Mn-specific SOD (*E. coli*) at pH 7.8 and 77 K. EPR spectra of Gly155Thr mutant Fe-SOD and Fe-SOD from *Ps. ovalis* reveal three intense signals in the 150 mT region, with effective g values equal to 4.84, 4.00, and 3.67 for the Gly155Thr mutant SOD and 4.81, 4.08, and 3.75 for the *Ps. ovalis* Fe-SOD. Further weak signals appear at low fields, with the corresponding effective g values of 9.9 and 9.3 for the mutant SOD and 9.9 and 9.2 for the *Ps. ovalis* SOD. These g values suggest that the electronic structures of the active sites are closely similar. They are consistent with those expected for high-spin iron(III) molecules with an $S = {}^5/_2$ ground state subject to zero-field splitting which resolves the 6-fold degeneracy into three Kramers doublets, with predominant spins of ${}^1/_2$, ${}^3/_2$, and ${}^5/_2$. In contrast to the similarity of the EPR spectrum of the Gly155Thr mutant Fe-SOD, that of Fe-SOD from wild-type *P. gingivalis* was somewhat different from that of Fe-specific Fe-SOD from *Ps. ovalis*. Wild-type Fe-SOD from *P. gingivalis* exhibited a $g = 4.35$ signal, a small broad peak around 8, and a small broad shoulder around 5.2, in addition to the g signals at 4.84, 4.05, and 3.70, which are the same

Table 3: Activities Measured by the Xanthine/Xanthine Oxidase System at pH 7.8 and Metal Contents of Fe- and Mn-SOD of the Wild-Type and the Gly155Thr Mutant from *P. gingivalis*[a]

sample	specific activity [units (mg of protein)$^{-1}$ (mol of Mn and/or Fe)$^{-1}$ (mol of subunit)$^{-1}$]	metal content (mol/mol of dimer)	
		Fe	Mn
Fe-reconstituted enzymes			
wild-type SOD	1598 ± 118	1.41 ± 0.04	0.004 ± 0.002
mutant SOD	3397 ± 311	1.40 ± 0.09	0.006 ± 0.002
Mn-reconstituted enzymes			
wild-type SOD	2653 ± 159	0.034 ± 0.046	1.49 ± 0.018
mutant SOD	304 ± 19	0.082 ± 0.025	1.69 ± 0.036

[a] Values are given as means ± the standard deviation.

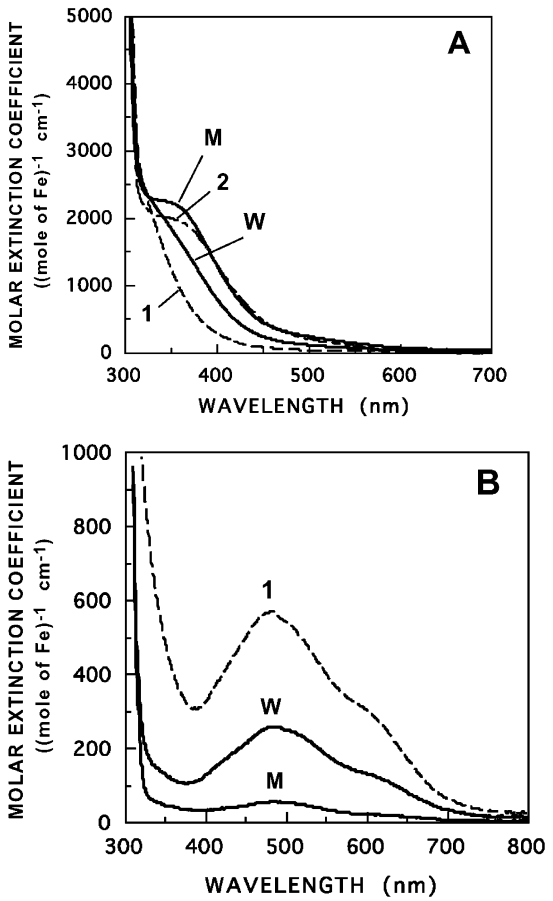

FIGURE 3: Comparison of the visible absorption profiles of Fe- and Mn-reconstituted wild-type and mutant *P. gingivalis* SODs. (A) Absorption spectra 1, 2, W, and M are for Fe-reconstituted Mn-SOD from *S. marcescens* (Mn-specific SOD), Fe-SOD from *Ps. ovalis* (Fe-specific SOD), Fe-reconstituted wild-type *P. gingivalis* SOD, and mutant SOD, respectively. (B) Absorption spectra 1, W, and M are for human Mn-SOD, Mn-reconstituted wild-type *P. gingivalis* SOD, and mutant SOD, respectively. The spectra were recorded in 10 mM potassium phosphate buffer (pH 7.8).

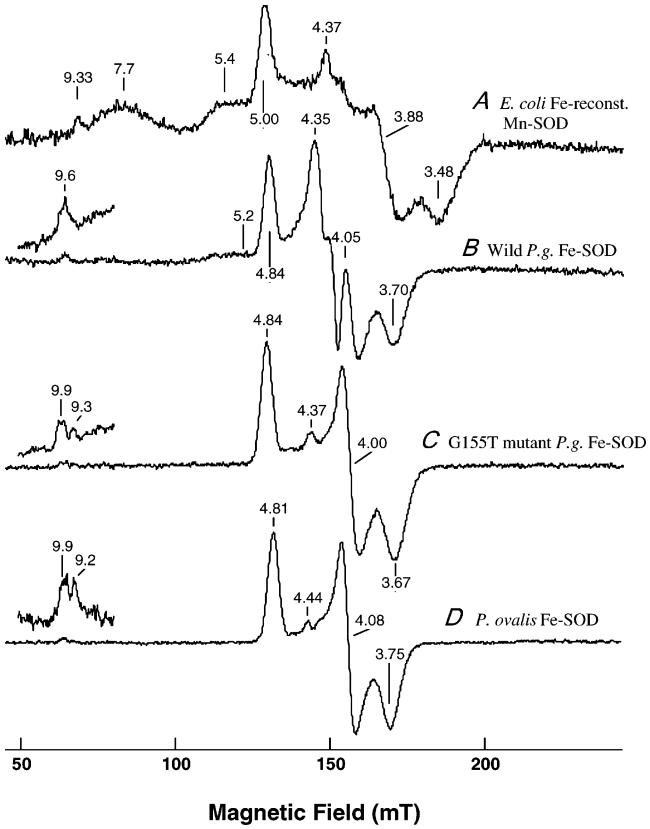

FIGURE 4: EPR spectra of Fe-SOD from wild-type and mutant *P. gingivalis*. (A) Fe-substituted Mn-SOD from *E. coli*. The amount of iron was 46 nmol in 200 μL of 10 mM potassium phosphate buffer (pH 7.8). The spectrum was recorded at 77 K with a modulation amplitude of 1 mT, a microwave power of 12 mW, and a gain of 400. (B) Fe-reconstituted SOD from wild-type *P. gingivalis*. The amount of iron was 16.6 nmol in 19 μL of 60 mM potassium phosphate buffer (pH 7.7). The spectrum was recorded at 4.5 K with a modulation amplitude of 0.63 mT, a microwave power of 1 mW, and a gain of 160. For measurement of the signals around 70 mT, a microwave power of 10 mW and a gain of 40 were used. (C) *P. gingivalis* Gly155Thr mutant Fe-reconstituted SOD. The amount of iron was 19.4 nmol in 250 μL of 160 mM potassium phosphate buffer (pH 7.7). The spectrum was recorded under the same conditions described above. (D) Fe-SOD from *Ps. ovalis*. The amount of iron was 14.7 nmol in 36 μL of 67 mM potassium phosphate buffer (pH 7.7). The spectrum was recorded under the same conditions described above, except at 8.8 K, a microwave power of 2.6 mW, and a gain of 79.

as those of the Gly155Thr mutant enzyme. The similar *g* signal at 4.37, and a more intense broad peak and shoulder, were also observed in Fe-substituted Mn-SOD from *E. coli* and *S. marcescens* [Figure 4A (*29*, *32*, *33*)]. Therefore, the cambialistic wild-type SOD from *P. gingivalis* seems to exhibit a mixed type EPR signal of Fe-specific SOD and Fe-substituted Mn-specific SOD.

Figure 5 shows EPR spectra of the wild-type and Gly155Thr mutant Mn-SODs from *P. gingivalis*, along with those of Mn-SOD from human and Mn-substituted Fe-SOD from *Ps. ovalis*. The spectra were recorded without reduction of manganese in the enzymes. Although the EPR spectra of the wild-type and the mutant SODs are similar to each other, those of the mutant SOD exhibited more apparent hyperfine structure of Mn^{2+}, where a sextet splitting with an a_{Mn} of 81 G is observed in the $g = 6.1$ feature (Figure 5C). The same type, but more intense signals, was observed in the

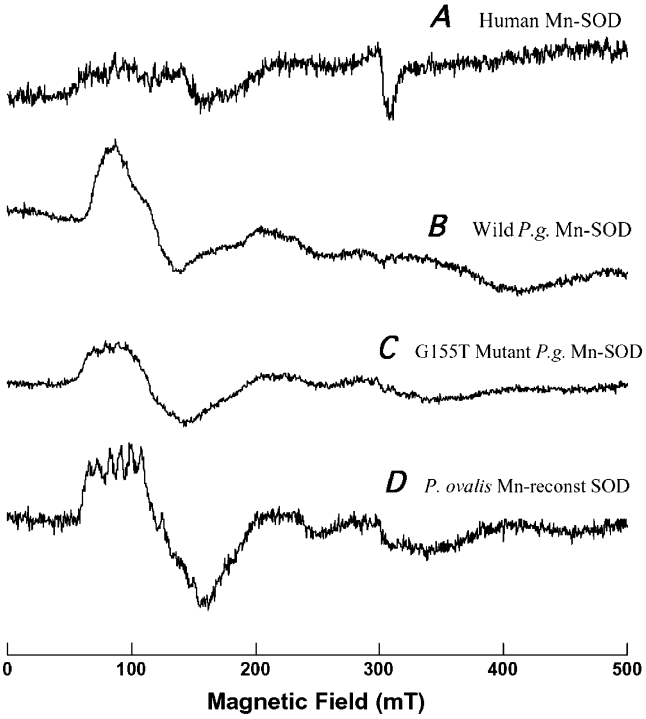

FIGURE 5: EPR spectra of Mn-reconstituted SOD from wild-type and mutant *P. gingivalis*. (A) Mn-SOD from human mitochondria. The amount of managnese was 19 nmol in 60 μL of 10 mM Tris-HCl buffer (pH 7.8). The spectrum was recorded at 4.4 K with a modulation amplitude of 0.63 mT, a microwave power of 1 mW, and a gain of 500. (B) Wild-type *P. gingivalis* Mn-reconstituted SOD. The amount of manganese was 44 nmol in 157 μL of 160 mM potassium phosphate buffer (pH 7.7). The spectrum was recorded at 4.5 K with a modulation amplitude of 0.63 mT, a microwave power of 1 mW, and a gain of 160. (C) Gly155Thr mutant *P. gingivalis* Mn-reconstituted SOD. The amount of manganese was 52 nmol in 200 μL of 130 mM potassium phosphate buffer (pH 7.7). The spectrum was recorded under the same conditions described above, except with a gain of 100. (D) Mn-substituted Fe-SOD from *Ps. ovalis*. The amount of manganese was 34 nmol in 100 μL of 10 mM Tris-HCl buffer (pH 7.8). The spectrum was recorded under the same conditions described above, except with a gain of 320.

spectrum of Mn-substituted Fe-SOD from *Ps. ovalis* (a_{Mn} = 83 G, g = 5.8, Figure 5D). The Mn^{2+} hyperfine structure was not resolved in the EPR spectrum of the wild-type SOD. No significant signal was observed in human Mn-SOD.

DISCUSSION

Characterization of the Mutant SOD. To elucidate the significance of glycine and threonine at position 155 in Mn-SODs and Fe-SODs, respectively, we used 73 Mn- and Fe-SODs from the Swiss-Prot database, including seven Archaea, 37 Eubacteriae, and 29 eukaryotes without redundancy of the species of origin. Amino acids at position 155 in *P. gingivalis* SOD, which are two amino acids before the third ligand Asp157, were analyzed. Among 49 Mn-SODs, 39 have glycine at position 155. The second most frequent amino acid is alanine (3 of 49). Among 24 Fe-SODs, 14 have threonine at position 155. The second most frequent amino acid is valine (5 of 24). Although the overall amino acid sequence of *P. gingivalis* SOD resembles those of Fe-SODs, it has glycine at position 155. Therefore, this glycine could be a candidate for the element that governs the cambialistic nature of this enzyme.

In PAGE, the mutant SODs exhibited a single major band (>95%) and a faster-moving minor band (<5%), with the same mobility as those of the wild-type SODs. This suggests that all the mutant SODs had the same gross structure as wild-type SODs, despite metal differences. The substitution of glycine 155 for threonine of *P. gingivalis* SOD changes the metal-specific activity of the enzyme from being slightly more efficient with Mn (1:1.7 for the Fe:Mn ratio) to being almost completely Fe-specific (1:0.089 for the Fe:Mn ratio, Table 3) based on the xanthine/xanthine oxidase system for the activity measurement. In conclusion, the conversion of glycine 155 to threonine resulted in a 19-fold increase in Fe-specific activity relative to Mn-specific activity. This is the first successful study in which the metal-specific activity was changed drastically by the site-directed mutation of a single amino acid located outside of the active site.

The visible absorption spectrum of the Gly155Thr mutant Fe-SOD exhibited almost the same spectrum as Fe-SOD from *Ps. ovalis* (Figure 3A), although the wild-type Fe-SOD exhibited an intermediate spectrum between those of Fe-specific and Mn-specific SODs. This evidence suggests that the iron environment of the mutant SOD is very close to that of the Fe-specific SOD. The evidence that the mutant Mn-SOD showed a very weak absorption at 480 nm, which resembles that of Mn-substituted Fe-specific SOD, supports this idea further. Vance and Miller (*34*) reported that Mn in Mn-reconstituted Fe-SOD from *E. coli* showed a higher reduction potential than that of Mn-SOD and presents an Mn^{2+} state as it was isolated. The reduction of Mn^{3+} of Mn-SOD to Mn^{2+} leads to a loss of the visible spectrum. From this line of evidence, we have concluded that Gly155Thr transforms the electronic environment of the metal and the ligands of the enzyme from that of a cambialistic type to an Fe-specific type.

High-spin iron(III) is a good probe for investigating electronic properties using EPR spectroscopy. The active site of the Gly155Thr mutant SOD appears to have almost the same electronic structure as the active site of Fe-specific SOD from *Ps. ovalis*, as shown in panels C and D of Figure 4. The signals near 150 mT could be assigned to high-spin ($^5/_2$) ferric iron with transitions in the middle Kramer's doublet (Ms = $\pm^3/_2$) in a field of nearly rhombic symmetry. The rhombicity, E/D, is estimated by fitting the effective g values to theoretical equations published by Wickman (*35*). E/D values are found to be 0.23 for both Gly155Thr mutant and wild-type SODs from *P. gingivalis* and 0.24 for *Ps. ovalis* Fe-SOD, defining similar distortions from axial symmetry. We have demonstrated the same unique features of the iron active site as observed in the Gly155Thr mutant SOD and *Ps. ovalis* Fe-SOD. Namely, the electronic structure for Fe-specific SODs must be present in all the active Fe sites of SODs to facilitate catalysis (*36*). The g = 4.3 signals in Fe-SOD from wild-type *P. gingivalis* could be attributed to two possible origins. One is the nonspecific iron that binds the enzyme other than the active site (*33*), which was found in Fe-SOD and Fe-substituted Mn-SOD (*33*, *37*). The other possibility is that the signal could be attributed to a specific orientation of the electron structure similar to that of the F^- binding Fe^{3+} site of Fe-SOD and Fe-substituted Mn-SOD from *E. coli* (*32*, *37*). We believe the second possibility is more probable, since the intensity of this signal has been changed by a pH difference with a complementary change

of the three rhombic signals, which suggests a conversion of the signals among each other (unpublished data). Increasing rhombicity is associated with near-octahedral geometry and six coordination for Fe^{3+} since the small departures from exact cubic symmetry are all similar in magnitude, resulting in an effective low level of symmetry for this site. The origins of the broad $g = 7-8$ peak and broad $g = 5-6$ shoulder are not clear at present, but a relatively axial spectrum arising within the $Ms = \pm 1/2$ doublet ($E/D \sim 0.05$) could be a candidate (*34*). Vance and Miller have suggested that the $g = 7-8$ similar peak and the $g = 5-6$ shoulder originate from a high-pH form of Fe^{3+} of the Fe-reconstituted Mn-SOD from *E. coli* (*33*).

The EPR spectrum of human Mn-SOD exhibited no significant signal (Figure 5A), since the signal of Mn^{3+} is difficult to observe by normal laboratory magnetic field and x-band microwave radiation in the presence of a sufficiently large zero field splitting, such as in the case of Mn-SOD (*38*). The spectra of Figure 5B−D are similar to the Mn^{2+} signals reported with reduced Mn-SOD and Mn-reconstituted Fe-SOD (*17*, *32*). Although the spectra of the wild-type Mn-SOD and the mutant Mn-SOD were very similar, the fine structure around 100 mT was observed only in the mutant enzyme and Mn-reconstituted Fe-SOD from *Ps. ovalis*. (Figure 5C,D). Recently, Un, Taberas, Cortez, Hiraoka, and Yamakura found that the Gly155Thr mutant Mn^{2+}-SOD exhibited almost the same high-field EPR spectrum as Mn^{2+}-substituted Fe-SOD from *E. coli*, but that of the wild-type Mn^{2+}-SOD was somewhat different. Un *et al*. speculate, using theoretical analysis, that a small difference in the distances from Mn^{2+} to OD1 of coordinate Asn157 between the wild-type and the mutant SODs may cause differences in the EPR parameters of the enzymes and also in the activity of both enzymes (unpublished data). Although differences in bond distances between each of the five ligands and metals in the wild-type Fe-SOD and the mutant Mn-SOD were not significant within our resolution of the X-ray structural study, the differences between metals and coordinate solvents or Asp157 were relatively larger in the mutant Mn-SOD than in the wild-type Fe-SOD compared with those between metals and other histidine ligands (Table 2). This evidence is consistent with the speculation born from the EPR parameters. However, further X-ray analysis with a higher resolution is required to prove the precise difference in the coordination distance.

The evidence from the absorption and EPR spectra, together with the results of the metal-specific activity of the mutant SOD, suggests that the mutation of glycine 155 to threonine results in a catalytic environment of the metal and a metal environment interaction of the cambialistic SOD which are almost the same as those of Fe-specific Fe-SOD.

Structural Bases of the Change in the Metal-Specific Activity. To determine the structural bases of the catalytic conversion of the mutant enzyme, we analyzed the structural differences between the X-ray structures of the wild-type Fe-SOD and mutant Mn-SOD enzymes. Two different explanations for the chemical bases of the metal-specific activities of Fe- and Mn-specific SODs have been proposed. These two explanations may not be mutually exclusive; rather, they may be complementary.

We reported that Fe-substituted Mn-SOD from *S. marcescens* shows a decrease in the enzyme activity with increasing pH with a p*K* of 7.0 (*29*), which is more than 2 units lower than that of Fe-SOD (*39*). This low p*K* value of Fe-substituted Mn-SOD reflects the low enzyme activity of the enzyme in the standard assay (pH 7.8), and confers the meta-specific activity on Mn-SOD. Whittaker *et al*. also reported a similar result for Fe-substituted Mn-SOD from *E. coli* (*32*). Recent structural studies of Fe-substituted Mn-SOD from *E. coli* have shown that the binding of the sixth ligand (OH^-) was observed at pH 8.5 but not observed in Fe- and Mn-SOD from *E. coli* at the same pH (*40*). Furthermore, the coordination number of Fe in the Fe form of cambialistic SOD from *Propionibacterium shermanii* changes from five to six with an increase in pH, coinciding with the pH-dependent decrease of the enzyme activity (*41*). This evidence suggests that the low p*K* value of the enzyme activity of Fe-substituted Mn-SOD may be caused by the higher affinity of the sixth ligand, probably OH^-, for the active site Fe, compared with that of Fe-SOD. Jackson *et al*. (*42*) support this idea with extensive spectroscopic and computational studies on Fe- and Mn-SOD. They suggest that hydroxide binding occurs at a pH lower than that of Tyr35 deprotonation in the Fe^{3+} form and possibly Mn^{2+} form of SODs and that this is the source of active-site p*K* in these forms of SOD. They support our idea that Fe^{3+}-reconstituted Mn-SOD also *binds* hydroxide at a pH lower than that of Fe^{3+}-SOD (*29*). They also have proposed that deprotonation of Tyr35 is a source of the active-site p*K* for the Fe^{2+} form and the Mn^{3+} form of SOD. Miller *et al*. (*43*) confirmed that the p*K* of the Fe^{2+} form of SOD was experimentally derived from Tyr35. Recently, Maliekal *et al*. (*44*) reported that the p*K* for Mn^{2+}-SOD from *E. coli* involves deprotonation of Tyr35 as well as the coordination sphere of Mn^{2+}, including hydroxide binding. These differences in the origin of p*K* values between Fe-SOD and Mn-SOD from *E. coli* were explained by the different electronic configurations of $Mn^{(2+/3+)}$ and $Fe^{(2+/3+)}$, such as the stronger hydrogen bonding between Gln146 and the coordinated solvent in Mn-SOD than between the analogous Gln69 (70 in *P. gingivalis* SOD) and coordinated solvent in Fe-SOD (*17*, *44*).

Vance and Miller have proposed that inactivation of metal-substituted SOD of Fe- and Mn-SOD from *E. coli* is due to inappropriate reduction potentials in metal-substituted enzymes; that is, $E° = 220$ mV for Fe-SOD and $E° = -240$ mV for Fe-substituted Mn-SOD (*34*), 290 mV for Mn-SOD, and >960 mV for Mn-substituted Fe-SOD (*31*). They suggest that a difference in the tuning properties in different types of SOD may cause inappropriate reduction potentials of the active site metals for catalysis of each half-reaction of the dismutation reaction of O_2^-, which should be within 200−300 mV. Recently, Yikilmaz *et al*. (*45*) suggested structural bases for tuning of the redox properties of the metals as follows. Since metal ion reduction is intimately coupled to proton uptake in Fe-SOD (*38*), the coordinate solvent is known as H_2O rather than OH^- in the reduced state of Fe-SOD. The shorter bond distance between coordinated OH^- and NE1 of Gln in Fe-substituted Mn-SOD compared to that in Fe-SOD (*11*, *17*, *45*) destabilizes coordinated H_2O versus OH^-, thus favoring the Fe^{3+} state and lowering the E_m in this enzyme.

Although we observed differences in the visible absorption spectra and EPR spectra between the wild-type and the

mutant Fe- and Mn-SODs, respectively, we found no large difference between the two enzymes with regard to the coordination structure of the enzyme. In the second sphere of the active site, however, insertion of a threonine residue between Trp123 and Trp125 resulted in movement of both tryptophan residues, as shown in Figures 1 and 2. Although no large difference is found between the wild-type and mutant SODs in the second sphere of the active site either, the differences shown below could provide a structural basis for metal-specific activity in each of the enzymes. Gln70 is an important residue; its side chain forms a second-shell hydrogen bond with the metal-coordinated solvent molecule and Tyr35 OH to make a hydrogen network system (Figure 1). In the wild-type structure, Gln70 makes four hydrogen bonds, involving both OE1 and NE1 of Gln70. NE1 of Gln70 is a donor in hydrogen bonds with the metal coordination solvent (2.93 Å) and the phenolic oxygen of Tyr35 (2.98 Å). OE1 of Gln70 is an acceptor in a hydrogen bond with NE1 of Trp123 (2.93 Å) and a weaker hydrogen bond with ND2 of Asn73 (3.33 Å) (Figure 2). In the mutant enzyme, the distance between OE1 of Gln70 and ND2 of Asn73 was extended to 3.56 Å, which is too far for hydrogen bonding. Instead, a new weak hydrogen bond between ND2 of Asn73 and NE1 of Trp123 (3.22 Å) appears. These differences in hydrogen bonds are caused by the difference in the position of Trp123 caused by the insertion of a threonine residue between Trp123 and Trp125. This additional hydrogen bond to NE1 of Trp123 may cause attenuation of the preexisting hydrogen bond between NE1 of Trp123 and OE1 of Gln70. The loss of one hydrogen bond and the attenuation of the preexisting hydrogen bond on OE1 of Gln70 could affect the two hydrogen bonds on NE1 of Gln70 through the delocalized π electron bond in the amide group of Gln70 (Figure 2). As a consequence, the donation of H of NE1 of Gln70 to the coordinated solvent and OH of Tyr35 might be weakened by the change in the hydrogen bond to OE1 of Gln70. The distances between the O of coordinate solvent and NE2 of Gln70 in the mutant Mn-SOD (3.37 Å) are longer than that of the wild-type Fe-SOD (2.93 Å) (Figure 2), which supports this idea. We could not find a difference in the bond distances between OH of Tyr35 and NE2 of Gln70 in the wild-type and mutant enzyme at the resolution of our X-ray analysis. However, if the hydrogen bond between OH of Tyr35 and NE2 of Gln70 were weakened in the mutant enzyme, the protonated form of OH of Tyr35 might be further stabilized and the p*K* of Tyr35 might be shifted to the higher pH as shown by Maliekal *et al.* (*43*) for Fe- and Mn-SOD from *E. coli*. Furthermore, this difference in the p*K* of Tyr35 may affect the binding of OH^- to the sixth coordination site in the Fe^{3+} form of the mutant SOD, which may contribute to the difference in the metal-specific activity of the mutant enzyme. Further X-ray structural analysis with higher resolution is required to confirm this idea.

Although the distance between the O of coordinate solvent and NE2 of Gln70 in the wild-type Fe-SOD (2.93 Å) is shorter than that of the mutant Mn-SOD (3.37 Å), the difference (0.44 Å) is not as short as that in Fe-SOD and Fe-substituted Mn-SOD (0.76 Å) proposed by Yikilmaz *et al.* (*45*). However, there is a possibility that the apparent increase in the distance in the mutant enzyme could tune the redox properties of the metal in the mutant enzyme in favor of iron rather than manganese, as shown by Yikilmaz *et al.* (*45*). This might be another way to confer Fe-specific activity on the mutant enzyme. The mutation of Asn73 and/or Trp123 would test the speculation described above. Although no other difference in the first sphere and the second sphere of the metal environment between the wild-type Fe-SOD and the mutant Mn-SOD was found by our X-ray crystallographic analyses, we cannot exclude the possibility that some small differences in the mutant SOD, which could not be realized by this resolution, could control the metal-specific activity. To elucidate this possibility, we are preparing an X-ray crystallographic study with higher resolution in our laboratory.

ACKNOWLEDGMENT

We thank Dr. Kimie Murayama and Dr. Hikari Taka (Juntendo University School of Medicine) for the measurements of LC−MS analysis. We also thank Tomoko Takei (Matsumoto Dental University) for technical assistance.

REFERENCES

1. Yamakura, F., and Suzuki, K. (1980) *J. Biochem. 88*, 191−196.
2. Ose, D. E., and Fridovich, I. (1976) *J. Biol. Chem. 251*, 1217−1218.
3. Brock, C. J., and Harris, J. I. (1977) *Biochem. Soc. Trans. 5*, 1533−1539.
4. Meier, B., Barra, D., Bossa, F., Calabrese, L., and Rotilio, G. (1982) *J. Biol. Chem. 257*, 13977−13980.
5. Martin, M. E., Byers, B. R., Olson, M. O. J., Salin, M. L., Arceneaux, E. L., and Tolbert, C. (1986) *J. Biol. Chem. 261*, 9361−9367.
6. Amano, A., Shizukuishi, S., Tsunemitsu, A., Maekawa, K., and Tsunasawa, S. (1990) *FEBS Lett. 272*, 217−220.
7. Yamakura, F., Rardin, R. L., Petsko, G. A., Ringe, D., Hiraoka, B. Y., Nakayama, K., Fujimura, T., Hikari, T., and Murayama, K. (1998) *Eur. J. Biochem. 253*, 49−56.
8. Parker, M. W., and Blake, C. C. F. (1988) *J. Mol. Biol. 199*, 649−661.
9. Ludwig, M. L., Metzger, A. L., Pattridge, K. A., and Stallings, W. C. (1991) *J. Mol. Biol. 219*, 335−358.
10. Borgstahl, G. E. O., Parge, H. E., Hickey, M. J., Beyer, W. F., Jr., Hallewell, R. A., and Tainer, J. A. (1992) *Cell 71*, 107−118.
11. Lah, M. S., Dixon, M. M., Pattridge, K. A., Stalling, W. C., Fee, L. A., and Ludwig, M. L. (1995) *Biochemistry 34*, 1646−1660.
12. Stoddard, B. L., Howell, P. L., Ringe, D., and Petsko, G. A. (1990) *Biochemistry 29*, 8885−8893.
13. Schmidt, M., Meier, B., and Parak, F. (1996) *J. Biol. Inorg. Chem. 1*, 532−541.
14. Sugio, S., Hiraoka, B. Y., and Yamakura, F. (2000) *Eur. J. Biochem. 267*, 3487−3495.
15. Yamano, S., and Maruyama, T. (1999) *J. Biochem. 125*, 186−193.
16. Hiraoka, B. Y., Yamakura, F., Sugio, S., and Nakayama, K. (2000) *Biochem. J. 345*, 345−350.
17. Schwartz, A. L., Yikilmaz, E., Vane, C. K., Vathyam, S., Koder, R. L., and Miller, A.-F. (2000) *J. Inorg. Biochem. 80*, 247−256.
18. Kunkel, T. A. (1985) *Proc. Natl. Acad. Sci. U.S.A. 82*, 488−492.
19. Leslie, A. G. W. (1998) *MOSFLM Users Guide*, MRC Laboratory of Molecular Biology, Cambridge, U.K.
20. Collaborative Computational Project No. 4 (1994) Programs for Protein Crystallography, *Acta Crystallogr. D50*, 760−763.
21. Matthews, B. W. (1968) *J. Mol. Biol. 33*, 491−497.
22. Brünger, A. T., Adams, P. D., Clore, G. M., DeLano, W. L., Gros, P., Grosse-Kunstleve, R. W., Jiang, J. S., Kuszewski, J., Nilges, M., Pannu, N. S., Read, R. J., Rice, L. M., Simonson, T., and Warren, G. L. (1998) *Acta Crystallogr. D54*, 905−921.
23. McRee, D. E. (1993) *Practical Protein Crystallography*, Academic Press, New York.
24. Ramakrishnan, C., and Ramachandran, G. N. (1965) *Biophys. J. 5*, 909−933.

25. McCord, J. M., and Fridovich, I. (1969) *J. Biol. Chem. 244*, 6049−6055.
26. Smith, P. K., Krohn, R. I., Hermanson, G. T., Malia, A. K., Gartner, F. H., Provenzano, M. D., Fujimoto, E. K., Goeke, N. M., Olson, B. J., and Klenk, D. C. (1985) *Anal. Biochem. 150*, 76−85.
27. Laskowski, R. A., MacArthur, M. W., Moss, D. S., and Thornton, J. M. (1993) *J. Appl. Crystallogr. 26*, 283−291.
28. Smith, F. G. (1963) in *Physical Geochemistry*, Addison-Wesley, Boston.
29. Yamakura, F., Kobayashi, K., Ue, H., and Konno, M. (1995) *Eur. J. Biochem. 227*, 700−706.
30. Yamakura, F. (1978) *J. Biochem. 83*, 849−857.
31. Vance, C. K., and Miller, A.-F. (2001) *Biochemistry 40*, 13079−13087.
32. Whittaker, M. M., and Whittaker, W. (1997) *Biochemistry 36*, 8923−8931.
33. Vance, C. K., and Miller, A.-F. (1998) *Biochemistry 37*, 5518−5527.
34. Vance, C. K., and Miller, A.-F. (1998) *J. Am. Chem. Soc. 120*, 461−467.
35. Wickman, H. H., Klein, M. P., and Shirley, D. A. (1965) *J. Chem. Phys. 42*, 2113−2117.
36. Renault, J. P., Verchere-Beaur, C., Morgenstern-Badarau, I., Yamakura, F., and Gerloch, M. (2000) *Inorg. Chem. 39*, 2666−2675.
37. Slykhouse, T. O., and Fee, J. A. (1976) *J. Biol. Chem. 251*, 5472−5477.
38. Fee, J. A., Shapiro, E. R., and Moss, T. H. (1976) *J. Biol. Chem. 251*, 6157−6159.
39. Bull, C., and Fee, J. A. (1985) *J. Am. Chem. Soc. 107*, 3295−3304.
40. Edward, R. A., Whittaker, M. M., Whittaker, J. W., Jameson, G. B., and Baker, E. N. (1998) *J. Am. Chem. Soc. 120*, 9684−9685.
41. Schmidt, M. (1999) *Eur. J. Biochem. 262*, 117−126.
42. Jackson, T. A., Xie, J., Yikilmaz, E., Miller, A.-F., and Brundld, T. C. (2002) *J. Am. Chem. Soc. 124*, 10833−10845.
43. Miller, A.-F., Padmakumar, K., Sorkin, D. L., Karapetian, A., and Vance, C. K. (2003) *J. Inorg. Biochem. 93*, 71−83.
44. Maliekal, J., Karapetan, A., Vance, C., Yikilmaz, E., Wu, Q., Jackson, T., Brounold, T. C., Spiro, T. G., and Miller, A.-F. (2002) *J. Am. Chem. Soc. 124*, 15064−15075.
45. Yikilmaz, E., Xie, J., Brunold, T. C., and Miller, A.-F. (2002*) J. Am. Chem. Soc. 124*, 3482−3483.

BI0349625